Bulletin of Mathematical Biology (2020) 82:34
https://doi.org/10.1007/s11538-020-00707-0

Society for Mathematical Biology

ORIGINAL ARTICLE

Toward Predicting the Spatio-Temporal Dynamics of Alopecia Areata Lesions Using Partial Differential Equation Analysis

Atanaska Dobreva[1] · **Ralf Paus**[2,3,4] · **N. G. Cogan**[5]

Received: 27 December 2018 / Accepted: 29 January 2020

Abstract
Hair loss in the autoimmune disease, alopecia areata (AA), is characterized by the appearance of circularly spreading alopecic lesions in seemingly healthy skin. The distinct spatial patterns of AA lesions form because the immune system attacks hair follicle cells that are in the process of producing hair shaft, catapults the mini-organs that produce hair from a state of growth (anagen) into an apoptosis-driven regression state (catagen), and causes major hair follicle dystrophy along with rapid hair shaft shedding. In this paper, we develop a model of partial differential equations (PDEs) to describe the spatio-temporal dynamics of immune system components that clinical and experimental studies show are primarily involved in the disease development. Global linear stability analysis reveals there is a most unstable mode giving rise to a pattern. The most unstable mode indicates a spatial scale consistent with results of the humanized AA mouse model of Gilhar et al. (Autoimmun Rev 15(7):726–735, 2016) for experimentally induced AA lesions. Numerical simulations of the PDE system confirm our analytic findings and illustrate the formation of a pattern that is characteristic of the spatio-temporal AA dynamics. We apply marginal linear stability analysis to examine and predict the pattern propagation.

Keywords Partial differential equations (PDEs) · Alopecia areata · Autoimmunity · Hair loss

1 Introduction

Autoimmune diseases constitute a heavy burden to society and require major health care resources. By 2003, close to 100 different autoimmune diseases had been rec-

Atanaska Dobreva received support from the Research Training Group in Mathematical Biology, funded by a National Science Foundation Grant RTG/DMS—1246991. Ralf Paus was supported in part by departmental start-up funds. N. G. Cogan received support from NSF CBET 1510743.

Extended author information available on the last page of the article

Published online: 24 February 2020

ognized (Cassell and Rose 2003), and the number of people suffering from them continues to increase every year. Some conditions have particularly high occurrence, such as type 1 diabetes (affecting the pancreas), celiac disease and inflammatory bowel disease (causing inflammation of the digestive tract), and multiple sclerosis (inflicting damage to the central nervous system) (Rose and Mackay 2013). Consequently, interest in investigations of autoimmune disorders through mathematical modeling and analysis has been growing.

In this study, we examine alopecia areata (AA), a model autoimmune disease that manifests with distinct hair loss patterns and represents actually one of the most common and most visible human autoimmune diseases (Gilhar et al. 2012, 2016; Paus et al. 2018). This disorder has not received as much attention in the field of mathematical modeling, since it is not fatal. AA, however, severely impacts quality of life of affected patients. In addition, the pathogenesis of AA shares some features with the pathomechanisms of more life-threatening or physically incapacitating autoimmune diseases (Gilhar et al. 2012, 2016), which impact organs and tissues that are not as accessible as hair follicles, for example inflammatory bowel disease, type I diabetes and rheumatoid arthritis (Bae et al. 2016; Wańkowicz-Kalińska et al. 2003; Bouma and Strober 2003; Skurkovich and Skurkovich 2003), and with the autoimmune depigmentation disorder, vitiligo (Harris 2013; Rork et al. 2016; Boniface and Seneschal 2019; Jimbo et al. 2020; Picardo and Taïeb 2019). Therefore, understanding and characterizing the interaction between the immune system and hair follicles will also shed light on other, harder to study diseases.

AA is classified as an organ-specific autoimmune disease since it attacks primarily hair follicles (HFs), the organs which produce hair, and the nail apparatus (Gilhar et al. 2012; Giordano and Sinha 2013; McElwee et al. 2013). In producing hair shafts, HFs constantly cycle through phases of growth (anagen), regression (catagen) and relative inactivity (telogen) (Paus and Cotsarelis 1999; Schneider et al. 2009). These cycling mini-organs present an excellent and highly accessible model system for spatio-temporally controlled changes in a complex biological system at the crossroads of developmental, systems and chronobiology (Al-Nuaimi et al. 2010, 2012, 2014; Plikus et al. 2015).

In AA, hair loss is caused by disrupting anagen and the induction of premature HF entry into catagen, along with the induction of major HF damage (HF dystrophy) that leads to the shedding of hair shafts, visible as hair loss (alopecia) (Gilhar et al. 2012). A critically required prerequisite for AA to develop is that the physiological immune privilege (IP) of HFs, i.e., an actively maintained immunoinhibitory tissue environment which normally prevents autoimmune attacks on the HF, is lost (Paus et al. 1993, 2005, 2018; Gilhar et al. 2012; Gilhar 2010; Ito 2010). This collapse of the HF's IP can be recreated in microdissected, organ-cultured human scalp HFs, and agents that induce, prevent its collapse, or restore HF IP can be tested in this ex vivo assay (Ito et al. 2004; Peters et al. 2007; Kinori et al. 2012; Bertolini et al. 2016).

For HFs, IP is established and maintained through the suppression of MHC class I molecules that present autoantigens and by the secretion of locally generated immunoinhibitors, such as transforming growth factor-β (TGF-β1 and 2), alpha-melanocyte-stimulating hormone (α-MSH) (Ito et al. 2004), calcitonin gene-related peptide (Kinori et al. 2012), vasoactive intestinal peptide (VIP) (Bertolini et al. 2016),

and cortisol (Ito et al. 2005a). These serve as important guardians of hair follicle immune privilege (HF IP) as they inhibit accumulation and/or activation of autoreactive immune cells in HFs (McElwee et al. 2013; Ito et al. 2004; Paus et al. 2005, 2008, 2018).

We previously modeled with ordinary differential equations (ODEs), the interactions between HFs and the immune system components and captured three states of a small cluster of homogeneous HFs: healthy, diseased and treatment (Dobreva et al. 2015). For the sake of an investigation more focused on understanding the complex temporal dynamics of immune cells and signals involved in AA, we assumed that HFs are in anagen and did not incorporate the hair cycle in the model. By simulating only the temporal dynamics of immune components, we were able to accurately show that a small cluster of HFs develops the disease if and when the populations of autoreactive lymphocytes expand sufficiently (Dobreva et al. 2015).

In a subsequent modeling effort with ODEs (Dobreva et al. 2017), we relaxed the assumption of anagen-only HFs and included HF cycling, connecting our earlier immune components system with equations that capture the human hair cycle (Al-Nuaimi et al. 2012). This allowed us to develop a temporal mathematical model for AA, which evolves the behavior of immune components along with the HF cycle dynamics, and thereby better reflects the complexity of disease events in vivo. Our results correctly predicted premature termination of the hair growth phase in response to an autoimmune reaction launched against HFs (Dobreva et al. 2017).

Our current study presents the development and analysis of a model of partial differential equations (PDEs) that aims to capture the spatio-temporal dynamics associated with AA. Hair loss in AA is characterized by distinct spatio-temporal patterns in which hair loss lesions appear, spread, coalesce or disappear again, leading to distinct clinical sub-phenotypes of the disease. Most commonly AA presents with round or oval hairless patches (Gilhar et al. 2012; Alkhalifah et al. 2010). Like for many other pattern formation phenomena associated with the appearance, spread and resolution of skin lesions in dermatological disease (Widelitz et al. 2006; Chuong et al. 2006), the biological basis of these distinct hair loss patterns in AA is poorly understood. However, as in other inflammatory skin diseases, it is highly plausible that one or several secreted, diffusible factors and migratory movements of immunocytes critically underlie these phenomena (Widelitz et al. 2006; Chuong et al. 2006).

2 Biological Background

The autoimmune development mechanism of AA is initiated by abnormally high production of pro-inflammatory cytokines, with a key role for interferon-gamma (IFN-γ), the most potent inducer of HF IP collapse, which not only exposes HFs to an attack by $CD8^+$ lymphocytes (Ito et al. 2004; Gilhar et al. 2012), but also induces premature HF entry into catagen and HF dystrophy (Ito et al. 2005b).

AA is primarily mediated by IFN-γ-secreting $CD8^+$ T cells, with an increasingly appreciated role for additional immunocytes, such as natural killer cells, which express NKG2D receptors that recognize a “danger” signal (MICA, ULBP3) expressed by stressed cells (Ito et al. 2008; Petukhova et al. 2010; Li et al. 2016). In particular,

autoreactive $CD8^+$ T cells/$NKG2D^+$ cells, assisted by $CD4^+$ T cells, are critically involved in the pathogenesis of AA and suffice to induce the disease (McElwee et al. 2013; Petukhova et al. 2010; Gilhar et al. 1998, 2002, 2012; Ito et al. 2008; Xing et al. 2014).

Lymphocytes are known to exhibit both random and directional movement. For example, T cells are guided toward places of inflammation in the body via cytokines and chemokines. Cytokines are immunoregulatory molecules that play a crucial role in the development, function and communication of all cells. Chemokines are a subfamily of cytokines capable of inducing chemotaxis in immune cells, that is, chemokines can attract and steer immune cells to move in a particular direction (Bae et al. 2016; Thelen and Uguccioni 2016). T cells also employ random movement to survey inflamed tissues in order to identify the cells that are compromised by pathogens, such as microbes and viruses, and need to be eradicated (Krummel et al. 2016; Rot and von Andrian 2004; Fowell 2016).

Directed migration of T cells in AA was investigated by Ito et al. (2013), who suggested that excessive chemokine secretion by lesional HFs may be the mechanism how inflammatory cell infiltrates are attracted to the HF. For the experimental study, scalp skin samples were obtained from healthy individuals and from hairless lesions of AA patients. The expression of CXCL10, a chemokine induced by IFN-γ (Luster and Ravetch 1987), was examined in healthy and diseased HFs. The results show that follicles from AA patches exhibit high expression of CXCL10 compared to those from normal skin. In addition, peripheral blood mononuclear cells were obtained from the AA patients and healthy control subjects. Using time-lapse images of cell migration, the investigators demonstrated that CXCL10 acts as a chemoattractant for AA-involved $CD4^+$ and $CD8^+$ T cells but not for the healthy control cells. Also, AA-involved $CD4^+$ and $CD8^+$ T cells showed higher expression of receptors for this chemokine compared to the T cells from healthy control individuals (Ito et al. 2013).

The Ito et al. (2013) study provides evidence that migratory motion of autoreactive lymphocytes in AA is strongly influenced by IFN-γ through the induction a of substance toward which the lymphocytes chemotact.

3 Model Construction

We develop a PDE model in one spatial dimension to describe how the patterns of hair loss in AA form. Based on the biological evidence presented in the previous section, it is suitable to describe the motility of AA-involved $CD4^+$ and $CD8^+$ T cells following the form of terms from the model for chemotaxis by Keller and Segel (1971). In formulating this model, both cellular motion impacted by interaction with a chemical signal and random motion unaffected by the signal are taken into account. Keller and Segel consider cells moving on a line from a position x the cells can move to the left or to the right. Then, the following approximation to $J(x)$, the net flux of cells per unit time in the positive x direction (increasing x), is derived

$$J(x) \approx -\mu \frac{\mathrm{d}b}{\mathrm{d}x} + \chi b \frac{\mathrm{d}c}{\mathrm{d}x}, \tag{1}$$

where $b(x)$ is the density of cells and $c(x)$ is the concentration of the chemoattractant in position x. The first term reflects random motility, and μ is the random motility (diffusion) coefficient. The second term reflects motion directed by the chemical substance, and χ is the chemotactic coefficient (Keller and Segel 1971). The following partial differential equation

$$\frac{\partial b}{\partial t} = -\frac{\partial}{\partial x} J(x) = -\frac{\partial}{\partial x}\left(-\mu \frac{\partial b}{\partial x} + \chi b \frac{\partial c}{\partial x}\right) \tag{2}$$

captures the dynamics of cell density $b(x, t)$, which depends on position and time (Keller and Segel 1971).

Since IFN-γ induces the chemokine CXCL10 (Luster and Ravetch 1987; Ito et al. 2013), as an acceptable simplification we assume that T cell motion in AA is able to respond to the IFN-γ concentration. In its current version, the PDE system does not include follicle cycling, and it reflects changes in time and in space of the key immune components involved in the pathomechanism of AA, IFN-γ (IFN), $CD8^+$ T cells/$NKG2D^+$ cells ($T8$) and $CD4^+$ T cells ($T4$). Figure 1 provides a visual representation of the diffusion and interaction between different model components, which is taking place in the scalp tissue. IFN-γ is produced by the immune cells ($p_{\mathrm{IFN}} T4 + p_{\mathrm{IFN}} T8$), and it diffuses $\left(D_{\mathrm{IFN}} \frac{\partial^2 \mathrm{IFN}}{\partial x^2}\right)$ and degrades ($-d_{\mathrm{IFN}}\mathrm{IFN}$). $CD8^+$ T cells/$NKG2D^+$ cells get activated in response to IFN-γ $\left(\frac{\alpha \mathrm{IFN}}{1+s}\right)$, proliferate with the help of $CD4^+$ T cells $\left(\frac{p_T \gamma T4 T8}{1+s}\right)$, and some of them die off ($-d_T T8 - \kappa_T (T8)^2$). The death term reflects natural death ($-d_T T8$) and concentration-dependent death due to inter-cell competition ($-\kappa_T (T8)^2$)). The lymphocyte activation and proliferation are suppressed by IP guardians. This inhibitory effect is reflected in the parameter s. Also, $CD8^+$ T cells/$NKG2D^+$ cells exhibit random motion $\left(D_{T8} \frac{\partial^2 T8}{\partial x^2}\right)$ as

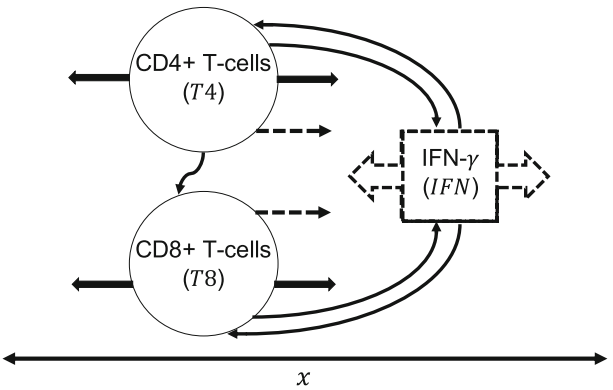

Fig. 1 Schematic illustration. T cells produce IFN-γ and get activated in response to IFN-γ. $CD8^+$ T cells proliferate with the help of $CD4^+$ T cells. IFN-γ diffuses. The spatial behavior of T cells includes random movement (solid arrows) and chemotaxis toward IFN-γ (dashed arrows). The diffusion and interaction between model components is taking place in the scalp tissue

well as motion directed up the concentration gradient in IFN-γ $\left(-\chi \frac{\partial}{\partial x}\left(T8 \frac{\partial \text{IFN}}{\partial x}\right)\right)$. CD4^+ T cells also become activated in response to IFN-γ $\left(\frac{\beta \text{IFN}}{1+s}\right)$ and proliferate $\left(\frac{p_T T4}{1+s}\right)$ under suppression from IP guardians. In addition, as with CD8^+ T cells/NKG2D^+ cells, the dynamics of CD4^+ T cells include natural and concentration-dependent death $(-d_T T4 - \kappa_T (T4)^2)$, random motion $\left(D_{T4} \frac{\partial^2 T4}{\partial x^2}\right)$, and chemotaxis $\left(-\chi \frac{\partial}{\partial x}\left(T4 \frac{\partial \text{IFN}}{\partial x}\right)\right)$. The equations capturing these events are given below. Model parameters along with their descriptions and nominal values are listed in Table 1. It should be noted that in addition to immunocyte activation by IFN-γ, α and β also reflect the levels of inactive CD8^+ and CD4^+ T cells, respectively, which are assumed to be constant. For a discussion on how parameters were estimated for the spatially homogeneous system, see Dobreva et al. (2015). The parameters corresponding to spatial dynamics were chosen based on information from the literature where available (see Table 1), and modulated to achieve alignment with experimental data on AA hairless patterns (Gilhar et al. 1998). Due to insufficient information about differences in the dynamics of CD4^+ and CD8^+ T cells during AA, we assume that parameters associated with activation, proliferation, death and motion are the same for the two populations of lymphocytes. We leave the exploration of potential differences in these parameters to future studies.

$$
\begin{aligned}
\frac{\partial *}{\partial t} &= \text{Production} - \text{Degradation} + \text{Diffusion} \\
\frac{\partial \text{IFN}}{\partial t} &= p_{\text{IFN}} T4 + p_{\text{IFN}} T8 - d_{\text{IFN}} \text{IFN} + D_{\text{IFN}} \frac{\partial^2 \text{IFN}}{\partial x^2} \\
\frac{\partial *}{\partial t} &= \text{Activation} + \text{Proliferation} - \text{Death} - \text{Chemotaxis} + \text{Diffusion} \\
\frac{\partial T8}{\partial t} &= \frac{\alpha \text{IFN}}{1+s} + \frac{p_T \gamma T4 T8}{1+s} - d_T T8 - \kappa_T (T8)^2 \\
&\quad - \chi \frac{\partial}{\partial x}\left(T8 \frac{\partial \text{IFN}}{\partial x}\right) + D_{T8} \frac{\partial^2 T8}{\partial x^2} \\
\frac{\partial T4}{\partial t} &= \frac{\beta \text{IFN}}{1+s} + \frac{p_T T4}{1+s} - d_T T4 - \kappa_T (T4)^2 \\
&\quad - \chi \frac{\partial}{\partial x}\left(T4 \frac{\partial \text{IFN}}{\partial x}\right) + D_{T4} \frac{\partial^2 T4}{\partial x^2}.
\end{aligned}
\tag{3}
$$

4 Experimental Data on Spatio-Temporal Dynamics of AA

An investigation which sheds light on the AA hairless patterns in association with the dynamics of T cells was conducted by Gilhar et al. (1998). After performing analysis of the PDE model, we compare our findings with the data and conclusions supplied by this experimental study.

Table 1 Values of PDE model parameters

Parameter	Description	Value	References
p_{IFN}	IFN production rate	$0.115\,\mathrm{pg\,day^{-1}}$	Estimation and Ito et al. (2004, 2005b)
d_{IFN}	IFN degradation rate	$1\,\mathrm{day^{-1}}$	Estimation and Ito et al. (2004, 2005b)
α	$T8$ activation rate in response to IFN	$0.08\,\mathrm{pg^{-1}}$	Estimated
β	$T4$ activation rate in response to IFN	$0.8975\,\mathrm{pg^{-1}}$	Estimated
s	HF IP guardians' strength of immunosuppression	0.1	Estimated
p_T	Proliferation rate of $T4$ and $T8$	$0.004\,\mathrm{day^{-1}}$	Mohri et al. (2001)
d_T	Natural death rate of $T4$ and $T8$	$0.05\,\mathrm{day^{-1}}$	Mohri et al. (2001)
κ_T	Concentration-dependent death rate of $T4$ and $T8$	$8 \times 10^{-7}\,(\mathrm{ml\,day})^{-1}$	Estimated
γ	Co-stimulation and proliferation stimuli from $T4$	$8 \times 10^{-5}\,\mathrm{ml^{-1}}$	Estimated
D_{IFN}	Diffusion coefficient of IFN	$10^{-2}\,\mathrm{cm^2\,day^{-1}}$	Estimated
D_{T8}	$T8$ diffusion coefficient	$10^{-3}\,\mathrm{cm^2\,day^{-1}}$	Estimation and Benechet et al. (2014) and Collins et al. (2016)
D_{T4}	$T4$ diffusion coefficient	$10^{-3}\,\mathrm{cm^2\,day^{-1}}$	Estimation and Benechet et al. (2014) and Collins et al. (2016)
χ	Chemotaxis coefficient for $T4$ and $T8$	$10^{-6}\,\mathrm{cm^2 day^{-1}}$	Estimated

Gilhar et al. (1998) is landmark study of pre-clinical AA research not only presented the first humanized mouse model for AA, but also demonstrated the critical importance of $CD8^+$ T cells for the induction of AA, exactly as previously postulated on theoretical grounds (Paus et al. 1993). Since then, this mouse model has been complemented and replaced by an optimized modification in which hair loss lesions can be induced even in previously healthy human scalp skin xenotransplanted onto immunocompromised mice after injection of suitably activated and pre-selected autologous lymphocytic cell populations (Gilhar et al. 2013, 2016).

Briefly, in the original humanized mouse model of AA (Gilhar et al. 1998) 2-mm scalp punch biopsies were obtained from AA patients. Some specimens were used to isolate scalp T cells, and 12 of the remaining ones were grafted onto mice with severe

combined immunodeficiency (SCID). Each mouse received 3 to 4 grafts. T cells were cultured with hair follicle homogenate (autoantigen) to become activated. On day 40, grafts were injected with a high dose of about 10^6 T cells. On day 82, mice were euthanized, and the grafts were analyzed. The results show that about 60 % of the grafts developed into hairless patches (Gilhar et al. 1998).

We consider the interval [0 cm, 1 cm] as the spatial domain, so that it can fit 5 grafts of size 2-mm, an amount close to the number of biopsies transplanted to each SCID mouse. Due to lack of information to describe the behavior of immune components at the domain boundaries, we prescribe periodic boundary conditions for the PDE model. HFs on the human scalp are arranged in collections, called follicular units. A unit can produce from one to five hairs, depending on how many follicles it contains. However, units of 4 or 5 follicles are rare. The mean distance between follicular units has been estimated to range from 1.0 to 1.4 mm (Jimenez and Ruifernández 1999). Also, there is approximately one follicular unit per mm^2 (Bernstein and Rassman 1997). So, a graft of size 2-mm contains a follicular unit with some interfollicular space.

5 Model Analysis

The behavior of PDEs is difficult to study. The task becomes even more complex when the equations contain nonlinear terms, and understanding and analyzing systems of nonlinear PDEs is particularly challenging. The model we formulated in Sect. 3 consists of coupled nonlinear PDEs and is classified as a reaction–diffusion system. Rather than engaging in qualitative theoretical study of existence and uniqueness or maximum/minimum points of a solution, we are more interested in analyzing the model behavior in light of the disease presentation in patients. The underlying observations we wish to investigate are the distinct spatial patterns and how they propagate. For this purpose, we utilize global linear stability analysis, numerical simulations, and marginal linear stability analysis.

5.1 Global Linear Stability Analysis

Global linear stability analysis (GLSA) is a classical way to look for patterns in the dynamics of reaction–diffusion PDEs without as well as with chemotaxis effects (Murray 2003a). With this method, we explore whether the AA patterns can be explained as an instability of a uniform solution (a steady state of the spatially homogeneous system), since this is how many patterns emerge in biological settings (Murray 1981, 2003b). For example, a reaction–diffusion–chemotaxis system, where spatial patterns evolve from a uniform state, has been used to describe the formation of spots and stripes on the skin of snakes. The precursors to pigment-producing cells are considered to initially be uniformly interspersed in the dermal skin of the developing snake embryo. Their dynamics are described with mitosis (logistic growth), random movement and chemotaxis, and the cells themselves synthesize the chemoattractant (Murray 2003c). With different parameter regimes, the model is able to generate a variety of snake patterns, which shows that interplay among the processes reflected in the equations

renders the uniform solution unstable and leads to spatially heterogeneous distribution of pigment-producing cells in the dermis (Murray 2003c).

As pointed out earlier, sufficiently large populations of autoreactive lymphocytes infiltrating HFs are considered drivers of the disease (Gilhar et al. 2012). So, the patterns observed as AA develops should be associated with an underlying spatio-temporal pattern in the levels of involved immune components. In other words, the hairless patches constitute regions where the amount of IFN-γ is high enough to trigger IP collapse, and immune cell aggregation and activation lies above a defined threshold value [on the order of 10^5 autoreactive cells (Alli et al. 2012; Gilhar et al. 1998)] that is sufficient in order to launch a successful destructive immune attack against HF cells. In our setting, it is suitable to consider a uniform solution which can be thought of as a susceptible state with the immune components being present throughout the domain but not yet elevated to an extent that would lead to disease manifestation. Such a non-zero steady-state accounts for the effect of external factors, such as skin damage or infection, which can be part of the initiation of AA onset. In applying GLSA, we derive a dispersion relation for the PDE model, and our results show that as a susceptible steady state of the spatially homogeneous system is perturbed with modes of different spatial frequency, a most unstable mode emerges, giving rise to a pattern.

5.1.1 Method Description

We carry out the following set of steps to derive a dispersion relation for the PDE model with periodic boundary conditions (Murray 2003a; Myerscough and Murray 1992):

1. *Determine a non-zero steady state of the spatially homogeneous system* A uniform solution (IFN*, $T8^*$, $T4^*$) s. t.

$$\begin{aligned}
\frac{\mathrm{dIFN}}{\mathrm{d}t} &= p_{\mathrm{IFN}} T4^* + p_{\mathrm{IFN}} T8^* - d_{\mathrm{IFN}} \mathrm{IFN}^* = 0 \\
\frac{\mathrm{d}T8}{\mathrm{d}t} &= \frac{\alpha \mathrm{IFN}^*}{1+s} + \frac{p_T \gamma T4^* T8^*}{1+s} - d_T T8^* - \kappa_T (T8^*)^2 = 0 \\
\frac{\mathrm{d}T4}{\mathrm{d}t} &= \frac{\beta \mathrm{IFN}^*}{1+s} + \frac{p_T T4^*}{1+s} - d_T T4^* - \kappa_T (T4^*)^2 = 0
\end{aligned} \tag{4}$$

2. *Perturb*

$$\begin{aligned}
&\mathrm{IFN} = \mathrm{IFN}^* + \epsilon \mathrm{IFN}_1(t,x); \quad T8 = T8^* + \epsilon T8_1(t,x); \\
&T4 = T4^* + \epsilon T4_1(t,x),
\end{aligned}$$

   where $\mathrm{IFN}_1(t,x) = Ae^{\lambda t + ikx}$; $T8_1(t,x) = Be^{\lambda t + ikx}$; $T4_1(t,x) = Ce^{\lambda t + ikx}$ and $0 < |\epsilon| \leq 1$.
3. *Linearize around the steady state and keep only ϵ contributions*
4. *Find λ as a function of the wave number k*

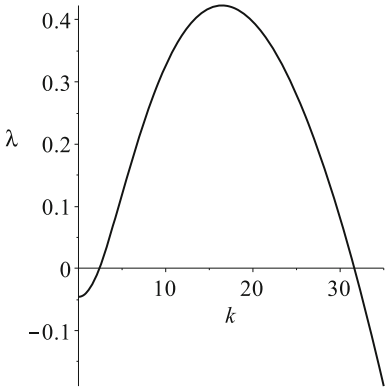

Fig. 2 Dispersion curve. Plot of the real part of the eigenvalue with largest magnitude as a function of the wave number k. The dispersion curve is generated using the parameter values from Table 1

We find the eigenvalues, λ, using $\det[\boldsymbol{M} - \lambda \boldsymbol{I}] = 0$. This leads to a cubic equation in λ which we solve in order to obtain a dispersion relation, that is, express λ as a function of the wave number k.

5. *Generate a dispersion curve by taking the eigenvalue λ with largest magnitude and plotting its real part against the wave number k* (Murray 2003a; Segel 1984).

5.1.2 Results

To find λ as a function of the wave number k and plot the dispersion curve, we carry out Steps (4) and (5) in Maple. The spatial perturbation to the uniform state is

$$e^{ikx} = \cos(kx) + i\,\sin(kx). \tag{5}$$

The wave number k shows how many cycles there are on an interval of length 2π. The spatial frequency is given by $\frac{k}{2\pi}$, and it represents the number of cycles on an interval of length 1. $\omega = \frac{2\pi}{k}$ is the wavelength and shows the length of each cycle.

Figure 2 presents the dispersion curve plot, created with the parameter values from Table 1. When $k = 0$, the real part of λ is negative, so the uniform steady state is stable to homogeneous perturbations, which is only the case for some particular combinations of parameters. For a discussion of the steady state's stability, please see Dobreva et al. (2015) where we conduct bifurcation analysis and show that the steady state is stable for the combination of parameters used here to generate the dispersion relation.

Figure 2 reveals that introducing diffusion and chemotaxis makes the uniform steady state unstable, so there are spatial perturbations that will grow and give rise to a pattern. In GLSA, the spatial perturbation to the uniform state is $e^{ikx} = \cos(kx) + i\,\sin(kx)$, so either $\cos(kx)$ or $\sin(kx)$ can be used as a specific form, and we work with $\sin(kx)$. As a perturbation grows, this would lead to a regular cyclical pattern of peaks and troughs in the levels of immune cells and IFN-γ. The maximally unstable mode is $k \approx 16$, which means that the dynamics of the PDE system are characterized by the development of a pattern with spatial frequency of $\frac{16}{2\pi} \approx 2.5$ and wavelength

of $\omega = \frac{2\pi}{16} \approx 0.39$. Spatial frequency of 2.5 means that we would have two and a half cycles on an interval of length 1, where the length of each cycle, given by the wavelength, would be 0.39.

The spatial domain for simulations in Sect. 5.2 is the interval [0 cm, 1 cm]. This domain allows to fit 5 grafts of size 2 mm, an amount close to the number of biopsies transplanted to each SCID mouse in the experimental study chosen for comparison (Gilhar et al. 1998). Since spatial frequency of 2.5 implies two and a half cycles, and there is a peak followed by a trough in each cycle, the pattern is characterized by three peaks and two troughs in the levels of immune components on the interval of length 1 cm. The length of one cycle is 0.39 cm, so each peak and each through occurs over length of approximately 0.2 cm. This is consistent with the size of an individual graft being such that it contains several follicular units together with some interfollicular space.

5.1.3 Effects of Parameter Variations on the Dispersion Relation

The dispersion curve in Fig. 2 is generated with values for the parameters as given in Table 1. In this section, we explore how parameter variations influence the dispersion relation and consequently the nature of arising patterns. The solid curves in the figures that we describe below correspond to the nominal parameter values from Table 1.

Figure 3 shows that increasing p_{IFN}, the rate at which $CD4^+$ and $CD8^+$ T cells produce IFN-γ moves the peak of the dispersion curve up and to the right. This means that higher IFN-γ level corresponds to a larger maximally unstable mode, which consequently gives a pattern with higher spatial frequency. Given the biologically relevant spatial domain, with regard to spacing of hair follicles (follicular units), $p_{\mathrm{IFN}} = 0.25$ is an extreme value that is not physiologically meaningful. Note that as p_{IFN} decreases, the peak of the dispersion curve moves down and to the left. For a value of p_{IFN} sufficiently small, for example 0.075, the curve falls below the k-axis, which signifies disappearance of the pattern. In the disease context, this means that as production of IFN-γ is downregulated, AA development will be suppressed.

Figure 4 shows that decreasing s, HF IP guardians' strength of immunosuppression, moves the peak of the dispersion curve up and to the right. This means that lower capacity of HF IP guardians to inhibit the activities of autoimmune components translates into a larger maximally unstable mode, which leads to a pattern with larger spatial frequency. However, as we can see there is a limiting value to how big the maximally unstable mode can get, and this value has a corresponding spatial frequency within the physiologically relevant range. As s decreases, the peak of the dispersion curve moves down and to the left, and for s sufficiently large, for example 1, the curve falls below the k-axis, making the pattern cease to exit. So, the progression of AA can be suppressed with endogenous HF IP guardians, such as TGF-β1/2, IL-10 and α-MSH, that are strong enough to counteract and halt the activities of autoimmune cells and signals.

Figure 5 shows how varying the diffusion coefficient of IFN, D_{IFN}, affects the dispersion curve. As we can see, lower D_{IFN}, which means IFN diffuses slowly, results in a pattern with larger spatial frequency. However, one the one hand, decreasing D_{IFN} too much would push the maximally unstable mode out of the biologically relevant

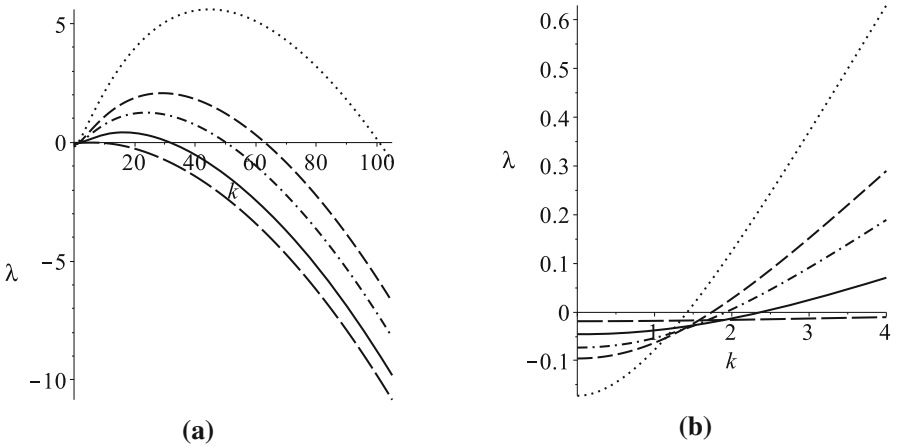

Fig. 3 **a** Broad view of the changes in the dispersion curve when p_{IFN} is varied. The values for the remaining parameters are taken from Table 1. Dotted curve: $p_{\text{IFN}} = 0.25$, Short dash curve: $p_{\text{IFN}} = 0.175$, Dash dot curve: $p_{\text{IFN}} = 0.15$, Solid curve: $p_{\text{IFN}} = 0.115$, Long dash curve: $p_{\text{IFN}} = 0.075$. **b** Zoom close to $k = 0$

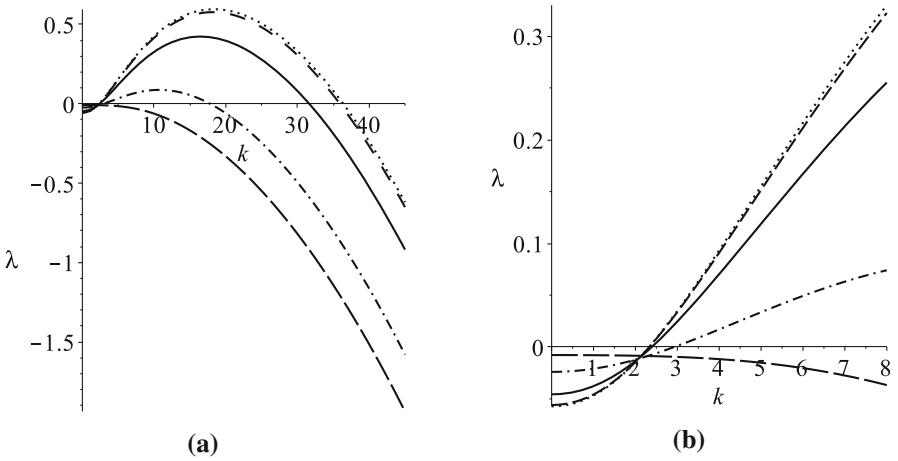

Fig. 4 **a** Broad view of the changes in the dispersion curve when s is varied. The values for the remaining parameters are taken from Table 1. Dotted curve: $s = 10^{-3}$, Short dash curve: $s = 10^{-2}$, Solid curve: $s = 10^{-1}$, Dash dot curve: $s = 0.5$, Long dash curve: $s = 1$. **b** Zoom close to $k = 0$

range. On the other hand, a significant increase in D_{IFN}, that is IFN diffusing too quickly, makes the pattern disappear.

Figure 6 shows the effects of changes in the parameters controlling random motion of $CD4^+$ and $CD8^+$ T cells, D_{T8} and D_{T4}. In this study, we make a simplifying assumption that $D_{T8} = D_{T4}$. As with D_{IFN}, we notice that very low values of D_{T8} and D_{T4}, that is T cells moving very slowly corresponds to a pattern with spatial frequency too large to be physically realistic in the context of hair follicle spacing over the scalp. Increasing D_{T8} and D_{T4}, meaning that if the random motion of T cells is too rapid, this causes the pattern to disappear.

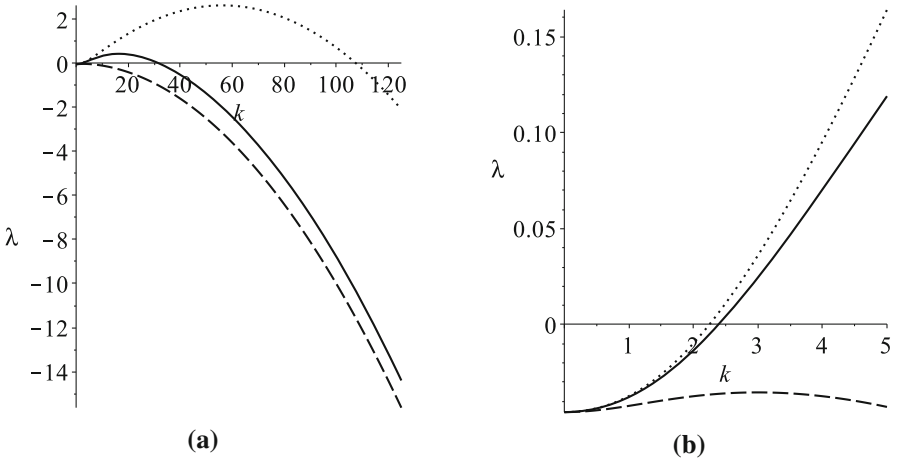

Fig. 5 **a** Broad view of the changes in the dispersion curve when D_{IFN} is varied. The values for the remaining parameters are taken from Table 1. Dotted curve: $D_{\text{IFN}} = 10^{-3}$, Solid curve: $D_{\text{IFN}} = 10^{-2}$, Dashed curve: $D_{\text{IFN}} = 10^{-1}$. **b** Zoom close to $k = 0$

Figure 7 shows how the dispersion curve is affected when the parameter controlling directed motion of $CD4^+$ and $CD8^+$ T cells, χ, varies. As χ increases a lot, the pattern that arises has too large of a spatial frequency to be relevant for interpretation in the case of AA. Lowering χ decreases the spatial frequency, and if χ falls sufficiently, the pattern vanishes.

In Table 2 in "Appendix", we present the changes brought about by variation in the remaining parameters. The parameters associated with immune cell proliferation, p_T and γ, have the following effects: higher values for those parameters lead to an increase in the spatial frequency and lower values cause the spatial frequency to decrease. However, within the range in which we vary p_T and γ, pattern disappearance does not come up as a result, even though the smallest value for p_T is 40 times lower than nominal level, and the smallest value for γ is 10 times lower than nominal level. We see a similar outcome with the parameter α, which reflects activation of $CD8^+$ T cells in response to IFN. Lowering the value to 5 times below nominal does not make the pattern cease to exit. On the other hand, with β, activation of $CD4^+$ T cells in response to IFN, decreasing the value to 2 times less than nominal causes the pattern to vanish.

Finally, as we can notice, as the death rate of immune cells (associated with parameters d_T and κ) increases, this leads to disappearance on the pattern, on the one hand. On the other hand, lower death rate increases the pattern's spatial frequency. The same effects are seen with d_{IFN}, the degradation rate of IFN.

5.2 Illustrative Simulations

We perform numerical simulations of the PDE model with periodic boundary conditions. The spatial domain is the interval [0 cm, 1 cm], and we use as an initial condition

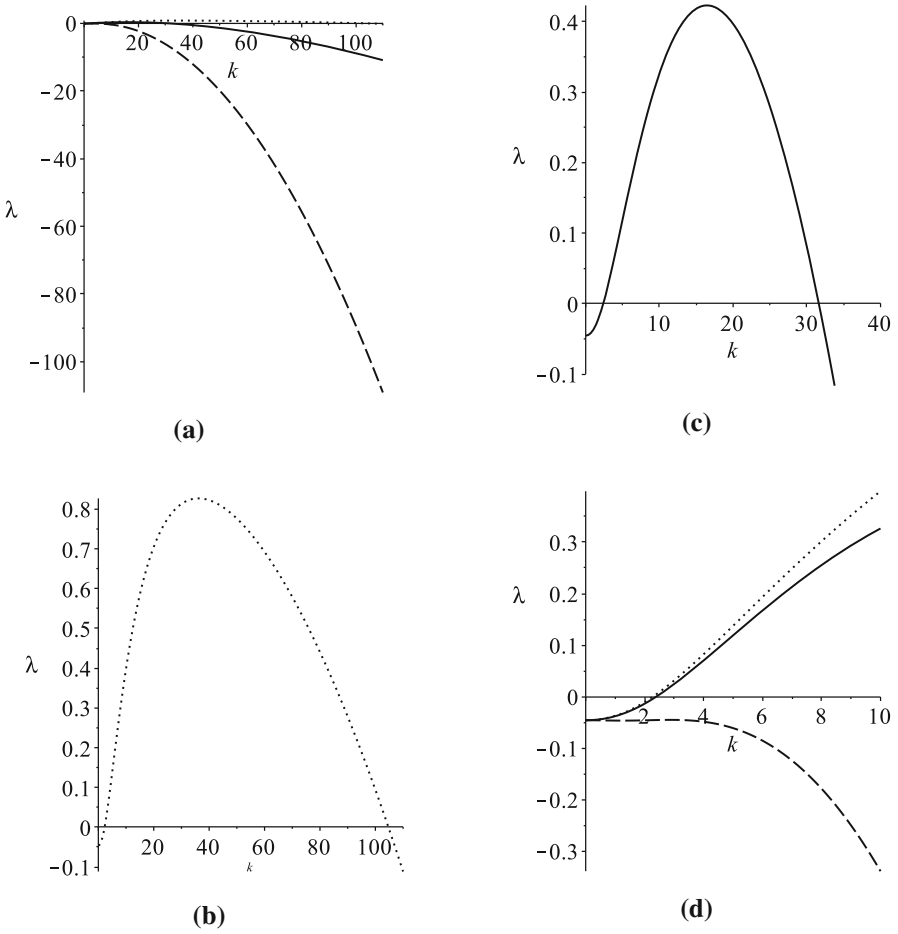

Fig. 6 **a** Broad view of the changes in the dispersion curve when D_{T8} is varied. The values for the remaining parameters are taken from Table 1. Dotted curve: $D_{T8} = D_{T4} = 10^{-4}$, Solid curve: $D_{T8} = D_{T4} = 10^{-3}$, Dashed curve: $D_{T8} = D_{T4} = 10^{-2}$. **a** Broad view of all dispersion curves. **b**, **c** Present individual plots of the dispersion curve with $D_{T8} = D_{T4} = 10^{-4}$ and $D_{T8} = D_{T4} = 10^{-3}$, respectively, to clearly show the presence of a maximally unstable mode. **d** Zoom close to $k = 0$

a globally perturbed steady state of the spatially homogeneous system. As explained earlier, this steady state can be thought of as a susceptible state where the immune components are elevated, but the disease has not yet induced a visible change in skin phenotype, i.e., hair loss. The spatial perturbations to the steady-state levels of IFN, $T8$, and $T4$ are proportional to $\epsilon \sin(16x)$, so that we can excite the most unstable mode. The value for ϵ is 10^{-2}.

To solve numerically the PDE system given in (3), we use the method of finite differences applying the upwind approach to the chemotaxis terms. We apply the Backward Euler method for the time discretization and a second centered difference quotient for the diffusion terms. In the chemotaxis terms, the first spatial derivative for IFN is

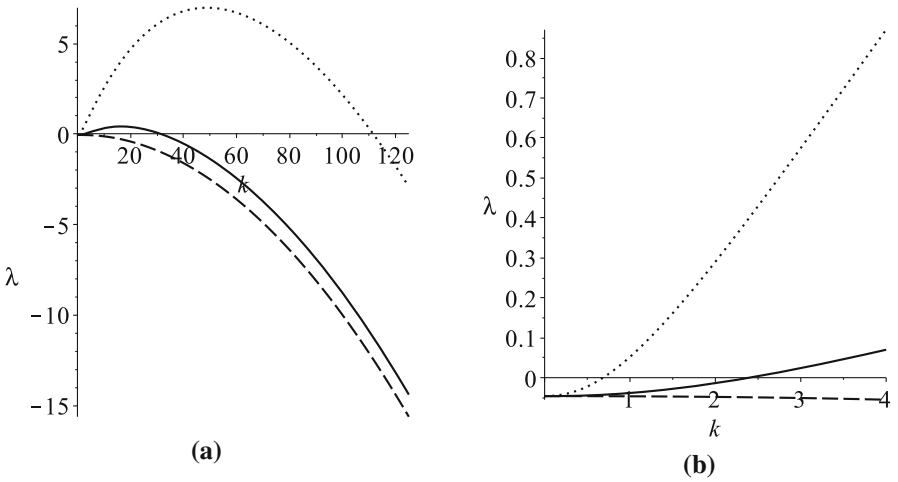

Fig. 7 **a** Broad view of the changes in the dispersion curve when χ is varied. The values for the remaining parameters are taken from Table 1. Dotted curve: $\chi = 10^{-5}$, Solid curve: $\chi = 10^{-6}$, Dashed curve: $\chi = 10^{-7}$. **a** Broad view of all dispersion curves. **b** Zoom close to $k = 0$

approximated with a centered difference. According to the upwind method (Pigozzo et al. 2011), we use a backward difference quotient for the first spatial derivative of $T8$ if the IFN derivative approximation is positive, and if the IFN derivative approximation is negative, we use a forward difference quotient for the first spatial derivative of $T8$. The chemotaxis terms in the equation for $T4$ are handled in the same way. We lag the nonlinear terms in the $T4$ and $T8$ equations, that is, we evaluate the nonlinear terms at the previous time step. The temporal step size used is $\Delta t = 0.001$, and the spatial step size is $\Delta x = 1/200$.

The results for IFN, $T8$, and $T4$ are shown in Fig. 8, and they illustrate the emergence of a pattern underlying the spatio-temporal dynamics for each immune component. The images in this figure come from the same simulation, and they give snapshots at three different times, $t = 5$ days, $t = 25$ days and $t = 55$ days to show how the patterns evolve. We can see that IFN, $T8$ and $T4$ exhibit the same sort of patterns, that is, places where IFN-γ expression is high are also places where the levels of immune cells are increased. The white spots are locations where the immune components become sufficiently elevated to lead to the development of hairless patches. The white spots correspond to space occupied by follicular units, and the black spots comprise interfollicular space.

The linearization for the PDE system, obtained from global linear stability analysis, holds up until about $t = 25$ days. The pattern we see in that time frame is consistent with the spatial frequency and wavelength found in the previous section. The analytic findings point to the emergence of three locations of length approximately 0.2 cm within which peaks in the immune components would occur, and the simulation results confirm this outcome. Later on, when the nonlinear effects in the PDE model are stronger, and the linearization no longer holds, the patterns take on a different form as the spatial frequency and wavelength change.

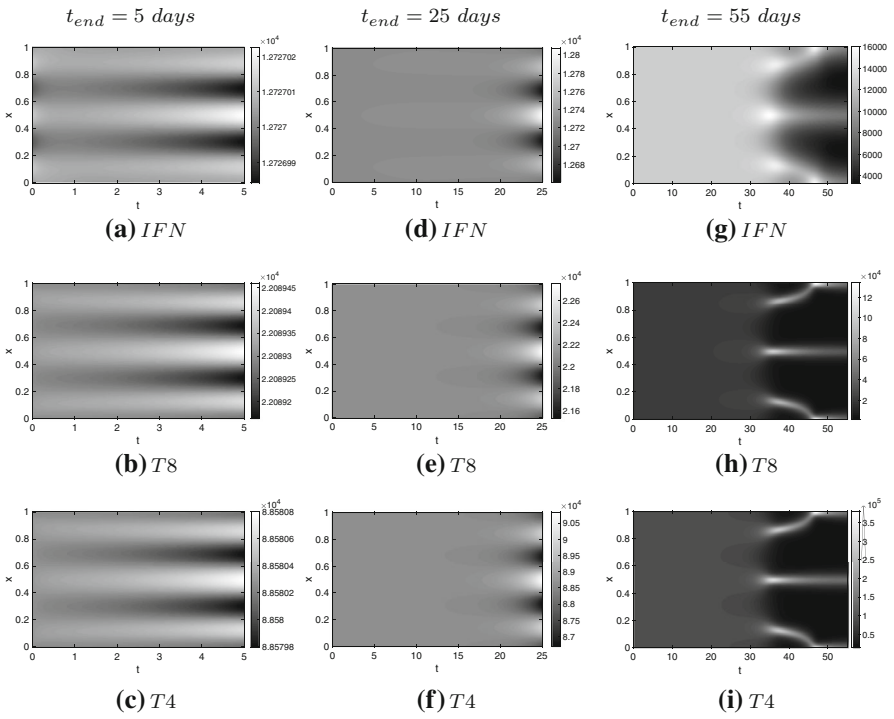

Fig. 8 Summary of results from simulating the PDE model with periodic boundary conditions on the interval [0 cm, 1 cm] using as an initial condition a susceptible steady state of the spatially homogeneous system (uniform solution) perturbed throughout the whole spatial domain. The parameter values are taken from Table 1. Note that in the cases of $t_{\text{end}} = 25$ days and $t_{\text{end}} = 55$ days a pattern characterizes the dynamics throughout the entire time frame. However, the pattern is not distinguishable for a portion of days in the beginning of the time period because the disturbances are much smaller at earlier days and undergo significant growth as time passes

5.3 Marginal Linear Stability Analysis

As noted earlier, GLSA is a way to examine whether the behavior of a PDE model entails the development of patterns (Murray 2003a). Our results from GLSA and numerical simulations show that distinct spatial patterns characterize the dynamics of interferon-γ, CD8$^+$ T cells, and CD4$^+$ T cells (Figs. 2, 8). However, in trying to better understand the progression of an AA patch, it is of great importance to also explore the propagation of the patterns as this closely relates with patch behavior, such as enlargement. While GLSA allows us to study patterns that form at the same time over the whole domain in response to a global perturbation (Murray 2003a), marginal linear stability analysis (MLSA) is a way to examine pattern propagation (Dee and Langer 1983). The MLSA method, developed by Dee and Langer (1983), focuses on the setting when a pattern emerges in an isolated region of the domain, as a result of a local disturbance, and spreads into the remaining space. The pattern appears behind a moving front, and one of the observations of interest is the speed of the front. Dee and Langer consider a pattern-forming nonlinear diffusion equation, and

as a way to estimate the front's propagation velocity they propose using the dispersion relation obtained from linearizing the equation about an unstable uniform state (Dee and Langer 1983).

According to Dee and Langer's argument, the small perturbation introduced locally would grow as it moves away from where it was initiated, taking the form $e^{\lambda(k^*)t+ik^*x}$, where k^* is the corresponding wave number (in the complex plane). Looking at the perturbation's behavior from a spatial coordinate $x = ct$ that moves in time, it should be possible to select a large enough c to place us at a position beyond the disturbance from where the perturbation would display as decaying in time. Marginal stability implies that the velocity v of the front, between a uniform region and a region with patterns, has a value such that the perturbation neither grows nor decays (Dee and Langer 1983). Even though a nonlinear diffusion equation is considered in Dee and Langer (1983), it has been shown that the MLSA method can be utilized for different types of nonlinear pattern-creating systems (Myerscough and Murray 1992; Ben-Jacob et al. 1985; Jensen et al. 1994; Cogan et al. 2012).

5.3.1 Method Description

In this section, we apply MLSA to explore the behavior of the PDE model in response to localized perturbations. Also, using the dispersion relation, we can find an estimate for the propagation velocity of the pattern. The estimate would be reliable only if, as the pattern propagates, the front moves at a constant rate. This comes from the MLSA assumption that at the leading edge of the front the introduced perturbation neither grows nor decays (Myerscough and Murray 1992; Dee and Langer 1983; Jensen et al. 1994; Cogan et al. 2012).

The perturbations we introduce are of the form $e^{\lambda(k)t+ikx}$. Separating $\lambda(k)$ and k into real (λ_r, k_r) and imaginary (λ_i, k_i) parts, we have

$$\lambda(k) = \lambda_r(k) + i\lambda_i(k), \quad k = k_r + ik_i. \tag{6}$$

So, we can rewrite the form of the perturbation as $e^{\lambda_r(k)t-k_ix}e^{i[\lambda_i(k)t+k_rx]}$. Requiring that the pattern front moves with uniform velocity (which is a real number) and its shape does not change as well as that the pattern front is stable to small changes in k, leads to the following conditions:

$$\begin{aligned} v &= \frac{\lambda_r(k)}{k_i} \\ v &= -\frac{\partial\lambda_i(k)}{\partial k_r} \\ 0 &= \frac{\partial\lambda_r(k)}{\partial k_r} \end{aligned} \tag{7}$$

where v is the propagation velocity of the pattern front (Myerscough and Murray 1992; Dee and Langer 1983; Jensen et al. 1994; Cogan et al. 2012).

5.3.2 Results

We perform the above described calculations in Maple in order to find k_r and k_i such that all three conditions are satisfied simultaneously. We generate surface plots in three dimensions of $\frac{\lambda_r(k)}{k_i}$, $-\frac{\partial\lambda_i(k)}{\partial k_r}$, and $\frac{\partial\lambda_r(k)}{\partial k_r}$, that is, we plot these quantities as functions of k_r and k_i. In addition, we plot the $k_i k_r$ plane where $\frac{\partial\lambda_r(k)}{\partial k_r}$ is 0. This way, we find the approximate location of the point where all three conditions hold simultaneously, and together with evaluations of the quantities of interest, we find $k_r = 12.525$ and $k_i = 12.844$. These values give propagation velocity $v = \pm 0.063$.

We next proceed to run simulations of the PDE model and compare with our analytically derived result for the propagation velocity. We again have periodic boundary conditions and use as an initial condition the susceptible steady state, which we perturb using the same form for the perturbation and the same maximally unstable mode as in GLSA. However, now we simulate the model on a larger spatial domain, the interval [0 cm, 10 cm], and introduce perturbations at a few locations in the domain. As Fig. 9 shows, we perturb in the middle of the interval and at each end. Part (a) illustrates that in the short term, while the linearization of the PDE system is valid, the pattern propagates with uniform velocity, which is well approximated by the magnitude of the slopes of the black lines. This magnitude is 0.063, the value for the propagation velocity that we obtained from the analytic method using the dispersion relation. As the locally introduced perturbations move in the larger spatial domain, on intervals of length 1 arises the same pattern that forms in GLSA (Fig. 8). As part (b) of Fig. 9 shows, at the later times, the approximation for the propagation velocity is not as good anymore, but this is expected since at those times the nonlinear effects take over, and the dispersion relation no longer holds.

5.3.3 Effects of IFN-γ and IP Guardians on Propagation Velocity

Finally, we explore how varying levels of IFN-γ and IP guardians influence the velocity of pattern propagation. For this purpose, we vary the parameters p_{IFN} and s. Note that for the simulation results in panels (a)–(c) in Figs. 10 and 11, the maximally unstable mode is different than the one for the results in (d)–(f). To make these figures, for each different parameter set we generated the dispersion relation to determine the maximally unstable mode, and this mode was used for the localized perturbations. The values of p_{IFN} and s used in Figs. 10 and 11 are explored earlier in Figs. 3 and 4, where we look at how parameter changes impact the dispersion relation. Our findings indicate that when p_{IFN} increases (Fig. 3), the peak of the dispersion curve moves, leading to a different maximally unstable mode compared to the nominal case. A similar outcome occurs when s decreases (Fig. 4).

Figure 10 presents a comparison between the patterns and their propagation velocities in the cases of normal and elevated production of IFN-γ, with simulations run out to 25 days. The velocities are given by the slopes of the black lines in the figure. IFN-γ synthesis is modulated by varying the parameter p_{IFN}. When the IFN-γ production is increased, the patterns propagate with larger velocity (0.111) than in the nominal case (0.063). Figures 12 and 13 (in "Appendix") show snapshots of how the patterns spread at 10, 15, 20, 25, 30, 40 and 50 days and confirm that larger production of IFN-

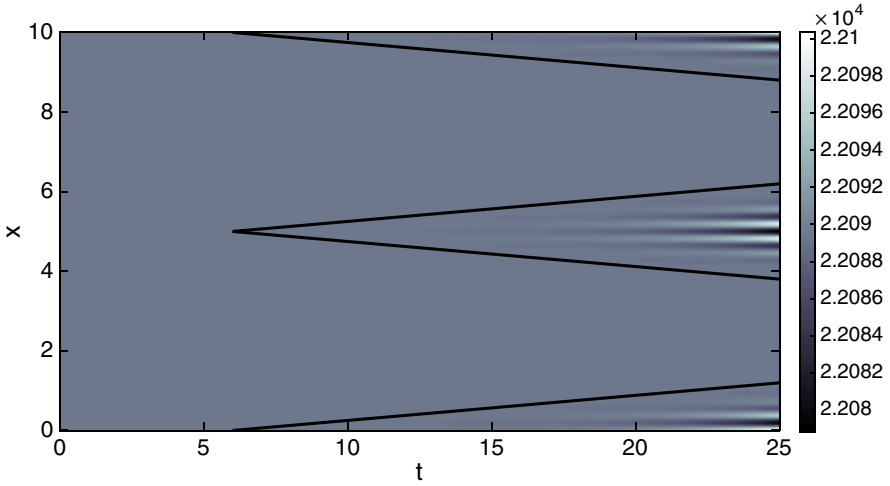

(a) $T8$, $t_{end} = 25$ days

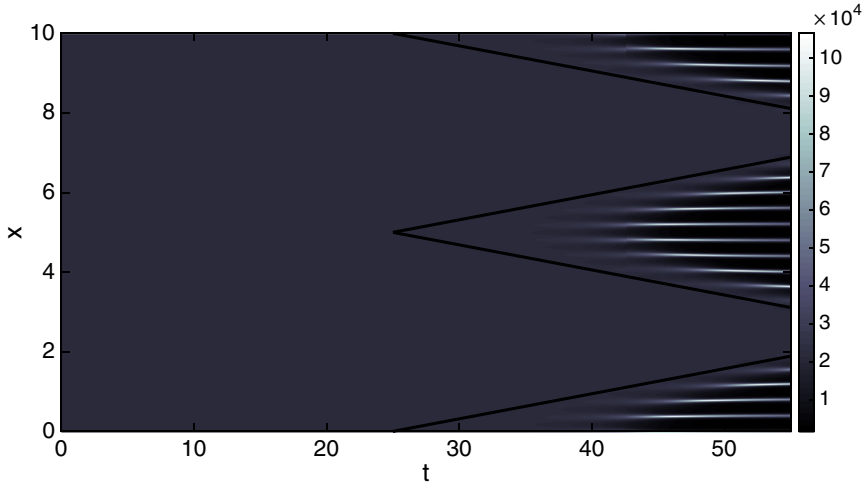

(b) $T8$, $t_{end} = 55$ days

Fig. 9 Results from linear marginal stability analysis. Parameter values used for this simulation are listed in Table 1. Magnitude of the slopes of the black lines is 0.063 (Color figure online)

γ leads to the patterns spreading more quickly. In the context of AA, this means faster enlargement of a hairless lesion. For further illustration, in Fig. 15 in "Appendix", we present the patterns at $t = 50$ days.

Figure 11 shows how the patterns and their velocities of spread compare between the cases of nominal level and decreased level of inhibitory strength of IP guardians. Strength of inhibition of IP guardians is modulated by varying the parameter s. Again, simulations are run out to 25 days. When the suppression effect of IP guardians is lower, the patterns spread with higher velocity (0.074) compared to the nominal case (0.063). Figures 12 and 14 (in "Appendix") show snapshots of how the patterns propagate at

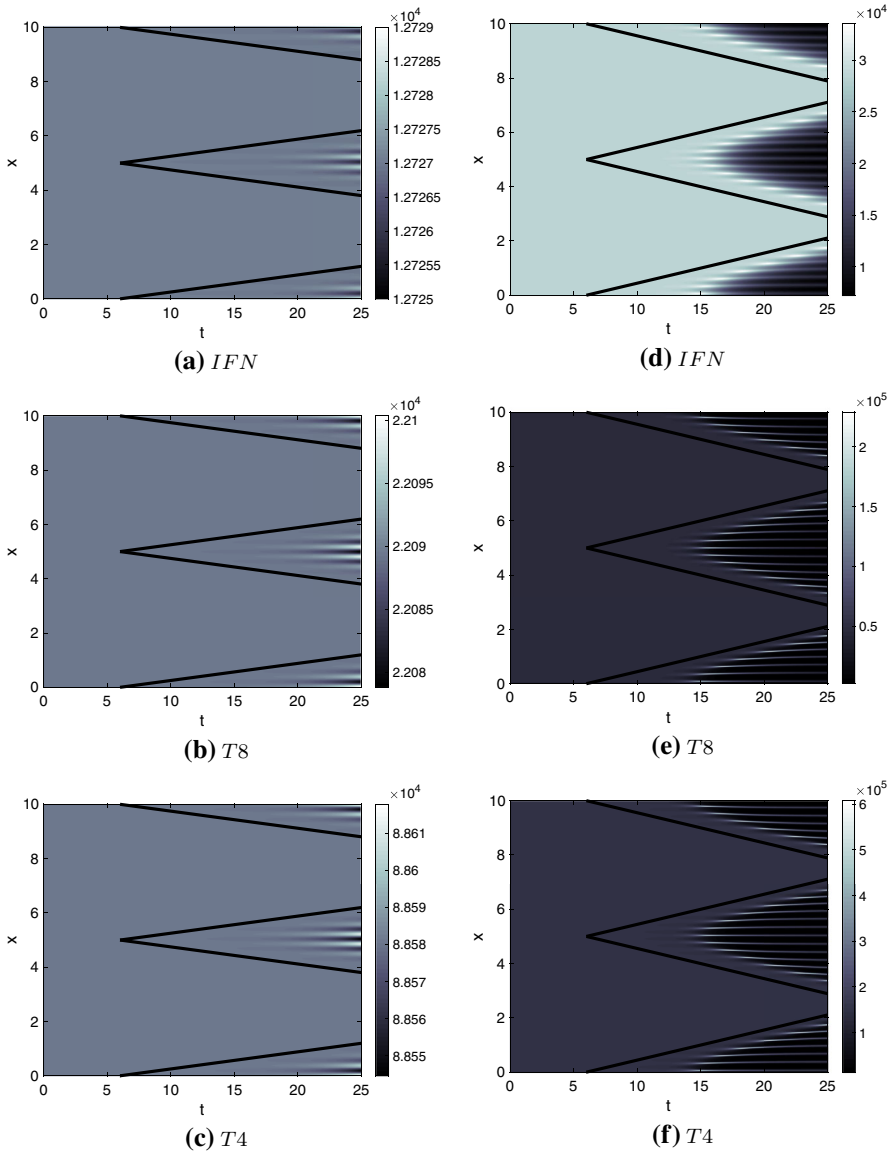

Fig. 10 t–time (in days), x–space (the interval [0 cm, 10 cm]). $t_{\text{end}} = 25$ days. Increasing the rate of production of IFN (p_{IFN}) leads to larger propagation velocity (slope of black lines). **a–c** $p_{\text{IFN}} = 0.115$, $s = 0.1$, velocity $= 0.063$. **d–f** $p_{\text{IFN}} = 0.15$, $s = 0.1$, velocity $= 0.111$. Note that in all images a pattern characterizes the dynamics throughout the entire time frame. However, in some images the pattern is not distinguishable for a portion of days in the beginning of the time period because the disturbances are much smaller at earlier days and undergo significant growth as time passes (Color figure online)

10, 15, 20, 25, 30, 40 and 50 days. These results also indicate that weakening the strength of immunosuppression of IP guardians increases the propagation velocity of

patterns, which means quicker patch expansion. For further illustration, Fig. 15 in "Appendix" shows the patterns at $t = 50$ days.

6 Discussion

In this paper, we construct a PDE model without hair cycle dynamics to describe the behavior in time and space of the main immune components involved in the development of AA, IFN-γ and $CD8^+$ T cells as primary players, and $CD4^+$ T cells as modifiers. Since AA attacks exclusively anagen HFs (Gilhar et al. 2012), it is acceptable and instructive to not include the hair cycle in the current context and to look only at anagen HFs.

The model manages to illustrate the emergence of a pattern, and the findings of our analysis are in agreement with the experimental results of Gilhar et al. (1998). The study reports that about 60 % of scalp biopsies transplanted onto SCID mice, where each scalp specimen is of size 2-mm, develop into hairless patches after receiving a high dose of activated T cells (Gilhar et al. 1998). Accepting this outcome as a pattern displayed in an emerging AA lesion, where lesion size is approximated by five 2-mm grafts, GLSA reveals that the PDE model is capable of generating such a pattern. Furthermore, simulations of the PDE model on [0 cm, 1 cm] confirm this outcome as they produce results characteristic of the AA pattern with consistent spatial and temporal scales, within a short-term time frame (about 25 days).

The data from the Gilhar et al. (1998) study cover only about 40 days, so more spatio-temporal data is needed on the dynamics of immune components at later times, in order to be able to analyze the model behavior in relation to AA at times past 40 days, where the nonlinear effects in the PDE model dominate and drive the behavior we observe.

Investigating how variations in parameters affect the dispersion relation and, therefore, the pattern, shows that some processes such as IFN-γ dynamics, activities of HF IP guardians, death rate of immune cells, and activation of $CD4^+$ T cells in response to IFN have influence over pattern emergence and disappearance. In addition, diffusion of IFN-γ, random motion of immune cells, and motion of immune cells directed by IFN-γ can also make the characteristic AA pattern arise or vanish. This means that these processes can give a way into disease suppression.

For example, when the parameter controlling IFN-γ synthesis is sufficiently small, this leads to disappearance of the pattern. In the disease context, this means that as the production of IFN-γ is downregulated, AA development will be suppressed. This result is perfectly in line with the recognized key role of IFN-γ in AA pathogenesis and underscores how well the model captures the biological and clinical reality of AA.

While IFN-γ degradation and diffusion as well as random motion of immune cells would not respond much to external influence, production of IFN-γ is a process that can be targeted clinically. Also, $CD4^+$ T cell activation in response to IFN-γ, immunosuppression via HF IP guardians, and the strength with which lymphocytes chemoattractant toward IFN-γ could potentially be modulated, thereby providing other possibilities for disease therapies.

Our model analysis shows that the progression of AA can be halted with endogenous HF IP guardians that are strong enough to suppress the actions of autoimmune cells and

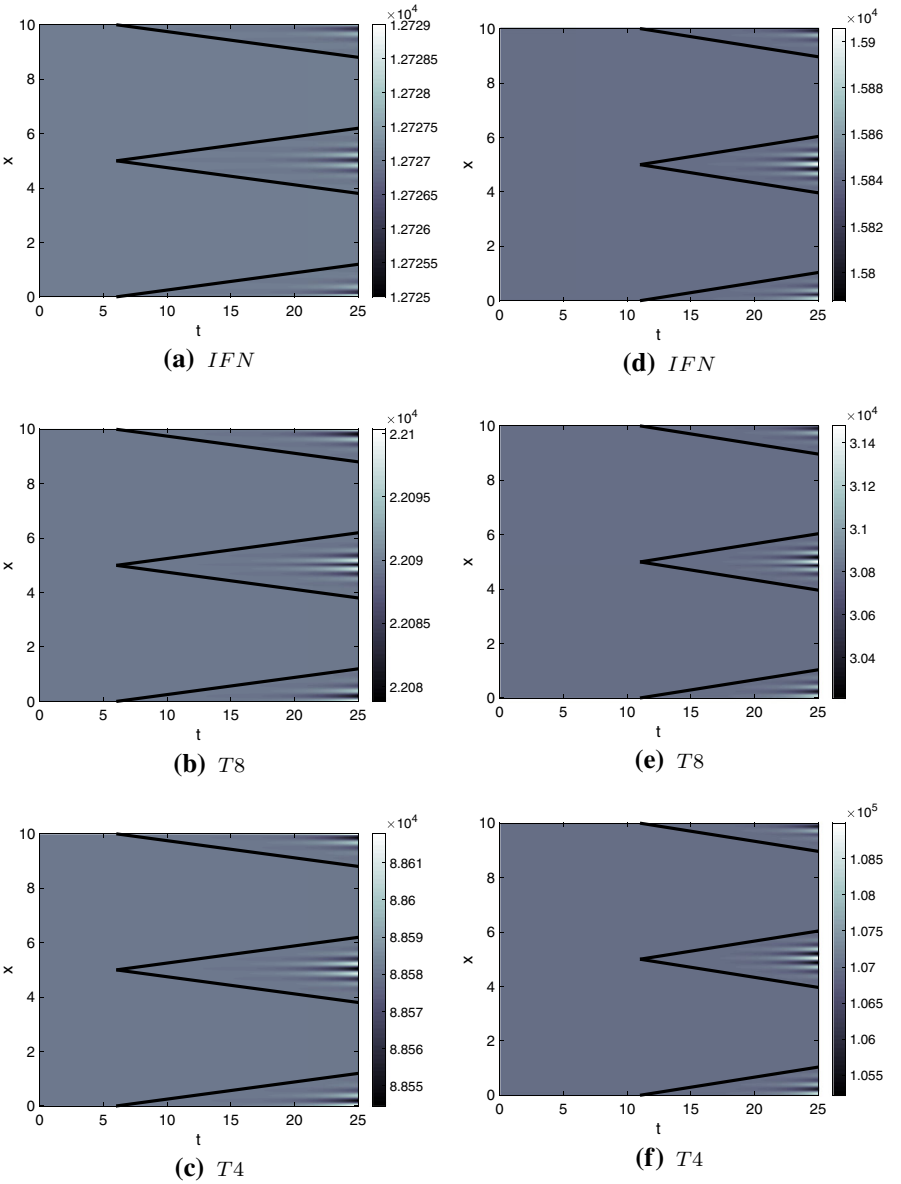

Fig. 11 t—time (in days), x—space (the interval [0 cm, 10 cm]). $t_{\text{end}} = 25$ days. Decreasing the inhibitory strength of IP guardians (s) leads to larger propagation velocity (slope of black lines). **a–c** $p_{\text{IFN}} = 0.115$, $s = 0.1$, Velocity = 0.063. **d–f** $p_{\text{IFN}} = 0.115$, $s = 0.01$, Velocity = 0.074. Note that in all images a pattern characterizes the dynamics throughout the entire time frame. However, in some images the pattern is not distinguishable for a portion of days in the beginning of the time period because the disturbances are much smaller at earlier days and undergo significant growth as time passes (Color figure online)

signals. This outcome suggests that therapeutic strategies for AA management which upregulate the intra- or perifollicular expression and secretion of IP guardians, such as TGF-β1/2, IL-10 and $\alpha-$MSH, would be expected to be very effective in assisting the HF restore its collapsed IP and to thus become protected against immune attack. Therefore, the current study supports earlier postulates that AA treatment strategy relying on HF IP guardians would be particularly effective (Paus et al. 1993, 2005, 2018; Gilhar et al. 2019b).

Another finding of our study is that reducing the sensitivity of T cell motion toward IFN-γ should suppress disease activity. This suggests that therapeutic interventions that make T cells less sensitive/receptive to IFN-γ stimulation (e.g., by downregulating IFNG receptor expression or by locally administering IFNG receptor antagonists) and/or that inhibit T cell migration deserve to be more systematically explored in future AA management. This is further supported by the fact that IFNG transcription is strongly upregulated in the hair bulb of AA patients (Kang et al. 2019).

The MLSA method allowed us to derive an estimate for the speed at which the pattern characteristic of AA would spread in a larger domain. Simulations of the model on [0 cm, 10 cm] confirm the velocity value predicted by the analytic approach, over a short-term time frame (about 25 days) where the linearization is a valid approximation to the nonlinear system, and the dispersion relation holds. Assuming that the propagation speed of the pattern could be interpreted as an indicator of the progression of a newly emerging AA lesion in the early stages of disease onset, our findings suggest that the patch would enlarge at a constant rate.

Analyzing the effects of IFN-γ and HF IP guardians on the pattern's propagation velocity shows that increased production of IFN-γ results in quicker spread, and, therefore, faster enlargement of an AA patch. Also, diminished immunosuppression from HF IP guardians leads to larger propagation velocity, which causes a lesion to expand more quickly. This further encourages a greater emphasis in future AA management on selectively targeting IFNG receptor-mediated signaling, rather than blocking signaling through many different JAK/STAT-dependent receptors (Gilhar et al. 2019a), and to focus more on up-regulating the intrafollicular expression of endogenous IP guardians (Paus et al. 2018; Gilhar et al. 2019b).

As pointed out in the Model Construction section, in this investigation we make a simplifying assumption that T cell movement in AA can respond to the concentration of IFN-γ. However, we recognize that it is actually chemokines that have the most profound impact on T cell motion, and as evidenced by the study of Ito et al. (2013), HF keratinocytes can secrete large amounts of chemokines, and chemokine receptor blockade can inhibit T cell migration and prevent AA in mice in vivo (Dai et al. 2016). So, a future development of the PDE model should incorporate activities of chemokines, as more data on their dynamics become available.

Also, other relevant but secondary immune cell populations, such as regulatory T cells, can be added to the model. However, since the specific role of regulatory T cells in the pathobiology of human AA remains ill-defined (Hamed et al. 2019; Speiser et al. 2019), these lymphocytes have purposely not been included in the current model, even though we recognize that they may have to be factored into a later, optimized model, which would enhance the relevance of the current model for other autoimmune skin diseases (Ujiie 2019).

Appendix

See Table 2 and Figs. 12, 13, 14 and 15.

Table 2 Effects of parameter variations on the dispersion relation

Parameter	Value	Maximally unstable mode	Maximum
d_{IFN}	0.5	30	2
	1	16	0.4
	2	0	− 0.005
α	0.02	13	0.2
	0.08	16	0.4
	0.4	26	1.3
β	0.44875	0	− 0.01
	0.8975	16	0.4
	4.4875	45	5.4
p_T	0.001	15	0.3
	0.004	16	0.4
	0.01	24	1.2
d_T	0.005	26	1.4
	0.05	16	0.4
	0.095	0	− 0.01
κ_T	4×10^{-7}	29	1.9
	8×10^{-7}	16	0.4
	8×10^{-6}	0	− 0.04
γ	8×10^{-6}	15	0.3
	8×10^{-5}	16	0.4
	16×10^{-5}	22	0.8

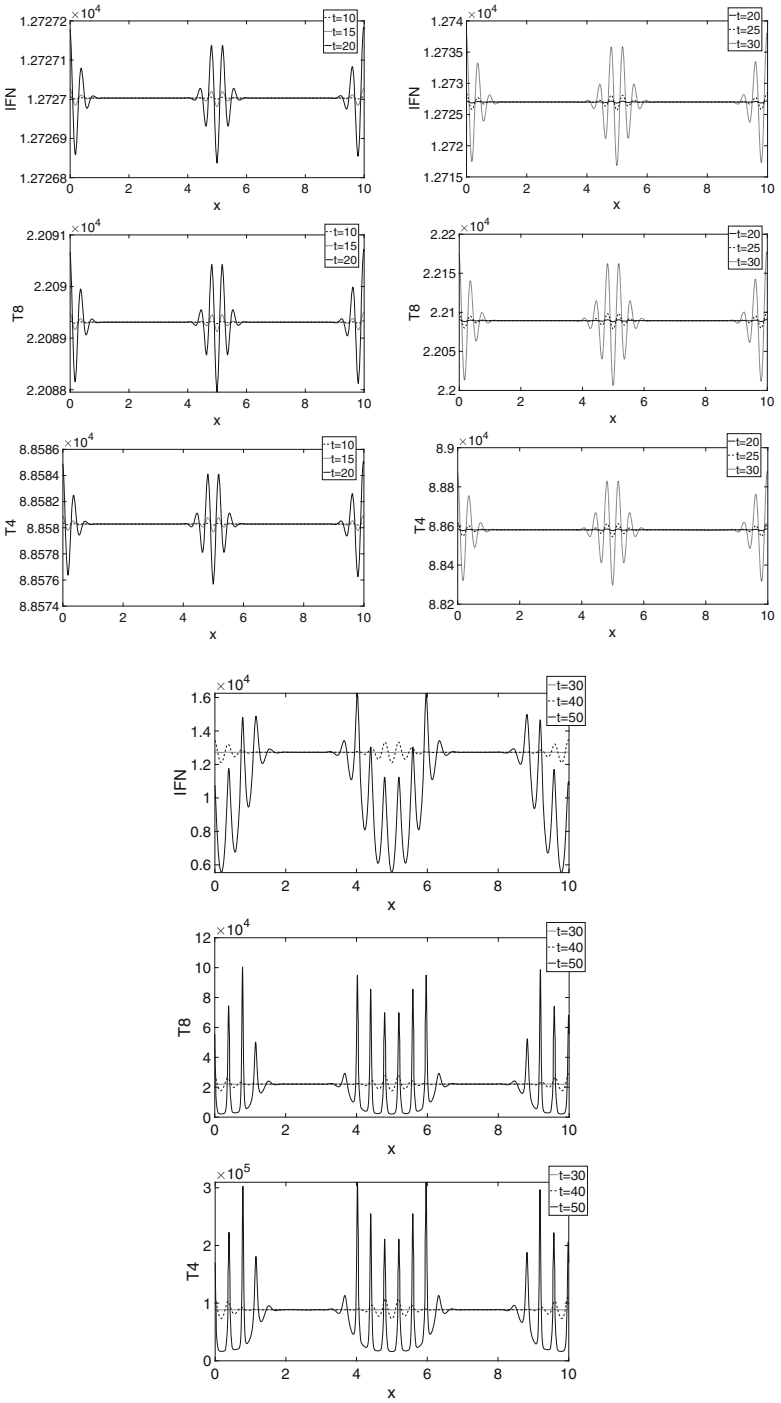

Fig. 12 t—time (in days), x—space (the interval [0 cm, 10 cm]). $p_{\mathrm{IFN}} = 0.115$, $s = 0.1$. Snapshots of the patterns' spread at 10, 15, 20, 25, 30, 40 and 50 days

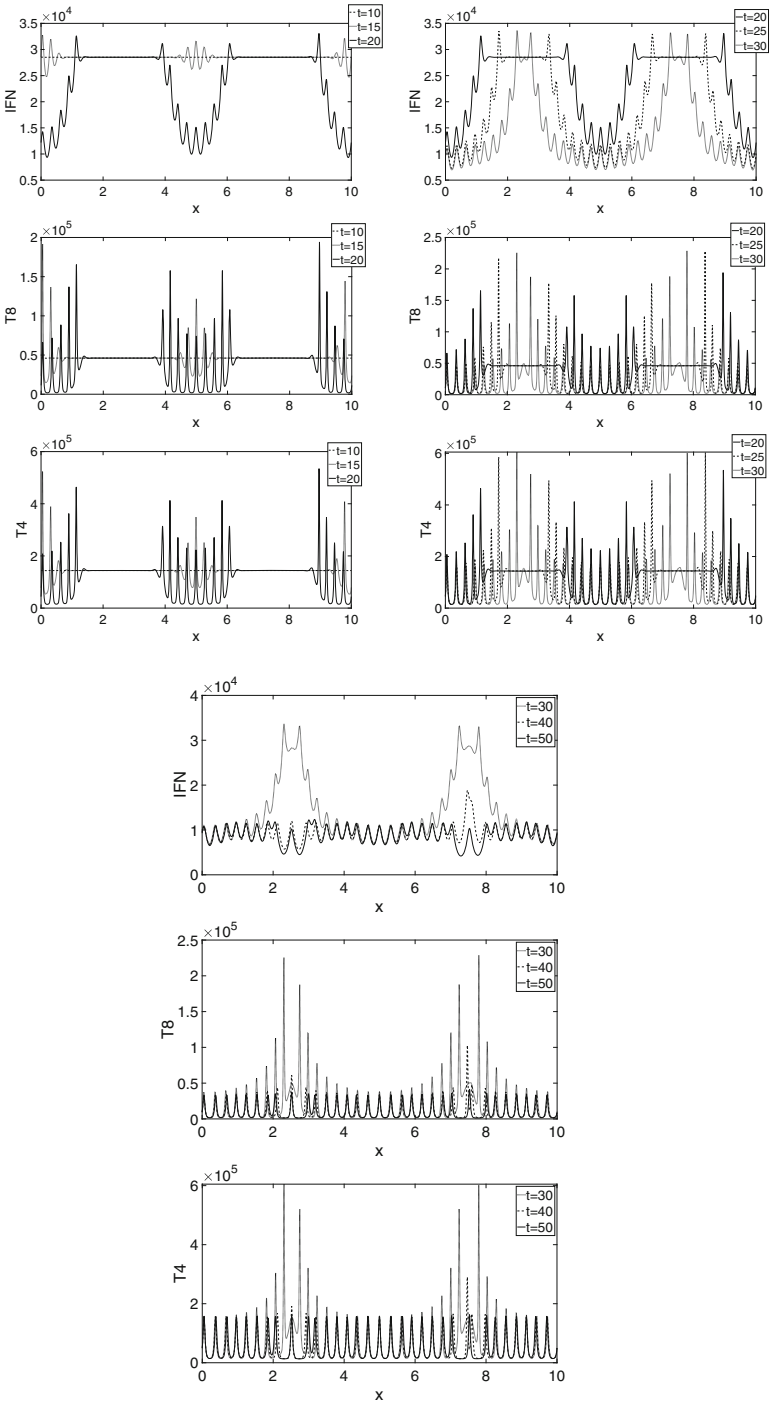

Fig. 13 t—time (in days), x—space (the interval [0 cm, 10 cm]). $p_{\mathrm{IFN}} = 0.15$, $s = 0.1$. Snapshots of the patterns' spread at 10, 15, 20, 25, 30, 40 and 50 days

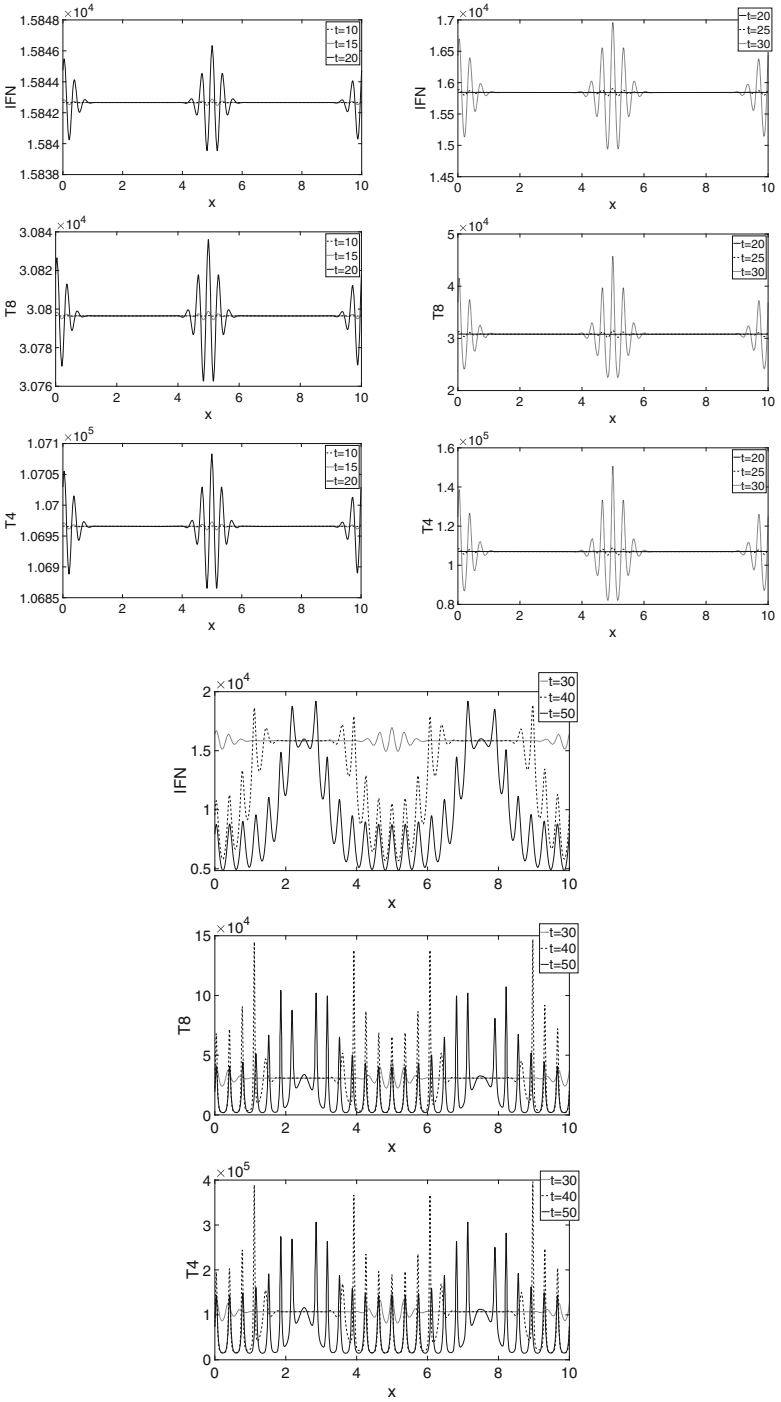

Fig. 14 t—time (in days), x—space (the interval [0 cm, 10 cm]). $p_{\mathrm{IFN}} = 0.115$, $s = 0.01$. Snapshots of the patterns' spread at 10, 15, 20, 25, 30, 40 and 50 days

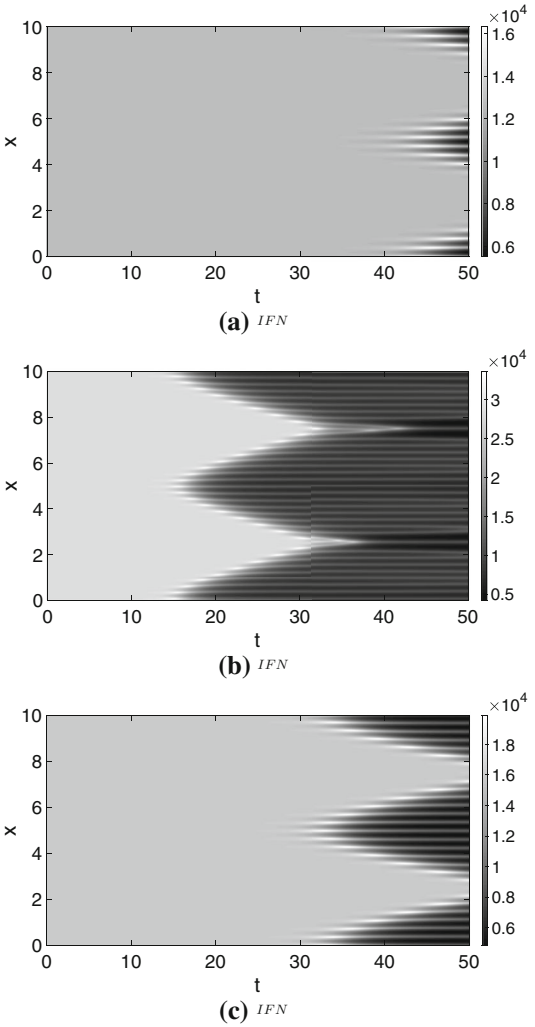

Fig. 15 t—time (in days), x—space (the interval [0 cm, 10 cm]). $t_{\text{end}} = 50$ days. **a** $p_{\text{IFN}} = 0.115$, $s = 0.1$; **b** $p_{\text{IFN}} = 0.15$, $s = 0.1$; **c** $p_{\text{IFN}} = 0.115$, $s = 0.01$. In each case, the patterns underlying the behavior of $T4$ and $T8$ are similar to the pattern exhibited by IFN, i.e., places where the IFN concentration is elevated are also places where the levels of $T4$ and $T8$ are increased

References

Alkhalifah A, Alsantali A, Wang E, McElwee KJ, Shapiro J (2010) Alopecia areata update: part I. Clinical picture, histopathology, and pathogenesis. J Am Acad Dermatol 62(2):177–188

Alli R, Nguyen P, Boyd K, Sundberg JP, Geiger TL (2012) A mouse model of clonal CD8+ T lymphocyte-mediated alopecia areata progressing to alopecia universalis. J Immunol 188(1):477–486

Al-Nuaimi Y, Baier G, Watson RE, Chuong CM, Paus R (2010) The cycling hair follicle as an ideal systems biology research model. Exp Dermatol 19(8):707–713

Al-Nuaimi Y, Goodfellow M, Paus R, Baier G (2012) A prototypic mathematical model of the human hair cycle. J Theor Biol 310:143–159

Al-Nuaimi Y, Hardman JA, Bíró T, Haslam IS, Philpott MP, Tóth BI, Farjo N, Farjo B, Baier G, Watson REB, Grimaldi B, Kloepper JE, Paus R (2014) A meeting of two chronobiological systems: circadian proteins Period1 and BMAL1 modulate the human hair cycle clock. J Invest Dermatol 134(3):610–619

Bae H, Barlow AT, Young H, Valencia JC (2016) Volume 2: molecular immunology. Cytokines and their receptors. In: Ratcliffe MJH, Colonna M, Elliott T, Mantovani A, Martin A (eds) Interferon-γ: an overview of its functions in health and disease, encyclopedia of immunobiology, 1st edn. Elsevier, Amsterdam, pp 494–500

Benechet AP, Menon M, Khanna KM (2014) Visualizing T cell migration in situ. Front Immunol. https://doi.org/10.3389/fimmu.2014.00363

Ben-Jacob E, Brand H, Dee G, Kramer L, Langer JS (1985) Pattern propagation in nonlinear dissipative systems. Phys D Nonlinear Phenom 14(3):348–364

Bernstein RM, Rassman WR (1997) The aesthetics of follicular transplantation. Dermatol Surg 23(9):785–799

Bertolini M, Pretzlaff M, Sulk M, Bähr M, Gherardini J, Uchida Y, Reibelt M, Kinori M, Rossi A, Bíró T, Paus R (2016) Vasoactive intestinal peptide, whose receptor-mediated signalling may be defective in alopecia areata, provides protection from hair follicle immune privilege collapse. Br J Dermatol 175(3):531–541

Boniface K, Seneschal J (2019) Vitiligo as a skin memory disease: the need for early intervention with immunomodulating agents and a maintenance therapy to target resident memory T cells. Exp Dermatol 28(6):656–661

Bouma G, Strober W (2003) The immunological and genetic basis of inflammatory bowel disease. Nat Rev Immunol 3(7):521–533

Cassell DK, Rose NR (2003) The encyclopedia of autoimmune diseases. Facts On File, Entries a-z, pp 3–9

Chuong CM, Dhouailly D, Gilmore S, Forest L, Shelley WB, Stenn KS, Maini P, Michon F, Parimoo S, Cadau S, Demongeot J, Zheng Y, Paus R, Happle R (2006) What is the biological basis of pattern formation of skin lesions? Exp Dermatol 15(7):547–564

Cogan NG, Donahue M, Whidden M (2012) Marginal stability and traveling fronts in two-phase mixtures. Phys Rev E 86(5):056204

Collins N, Jiang X, Zaid A, Macleod BL, Li J, Park CO, Haque A, Bedoui S, Heath WR, Mueller SN, Kupper TS, Gebhardt T, Carbone FR (2016) Skin $CD4^+$ memory T cells exhibit combined cluster-mediated retention and equilibration with the circulation. Nat Commun 7, Article number: 11514

Dai Z, Xing L, Cerise J, Wang EH, Jabbari A, de Jong A, Petukhova L, Christiano AM, Clynes R (2016) CXCR3 blockade inhibits T cell migration into the skin and prevents development of alopecia areata. J Immunol 197(4):1089–1099

Dee G, Langer JS (1983) Propagating pattern selection. Phys Rev Lett 50(6):383–386

Dobreva A, Paus R, Cogan NG (2015) Mathematical model for alopecia areata. J Theor Biol 380:332–345

Dobreva A, Paus R, Cogan NG (2017) Analysing the dynamics of a model for alopecia areata as an autoimmune disorder of hair follicle cycling. Math Med Biol 35(3):387–407

Fowell DJ (2016) Volume 3: activation of the immune system. T cell activation. In: Ratcliffe MJH, Defranco A, Miyasaka M, Mosmann T (eds) Modification of T cell functions at sites of infection and inflammation, encyclopedia of immunobiology, 1st edn. Elsevier, Amsterdam, pp 336–343

Gilhar A (2010) Collapse of immune privilege in alopecia areata: coincidental or substantial? J Invest Dermatol 130:2535–2537

Gilhar A, Ullmann Y, Berkutzki T, Assy B, Kalish RS (1998) Autoimmune hair loss (alopecia areata) transferred by T lymphocytes to human scalp explants on SCID mice. J Clin Invest 101(1):62–67

Gilhar A, Landau M, Assy B, Shalaginov R, Serafimovich S, Kalish RS (2002) Mediation of alopecia areata by cooperation between $CD4^+$ and $CD8^+$ T lymphocytes: transfer to human scalp explants on $Prkdc^{scid}$ mice. Arch Dermatol 138(7):916–922

Gilhar A, Etzioni A, Paus R (2012) Medical progress: alopecia areata. N Eng J Med 366(16):1515–1525

Gilhar A, Keren A, Paus R (2013) A new humanized mouse model for alopecia areata. J Invest Dermatol Symp Proc 16(1):S37–S38

Gilhar A, Schrum AG, Etzioni A, Waldmann H, Paus R (2016) Alopecia areata: Animal models illuminate autoimmune pathogenesis and novel immunotherapeutic strategies. Autoimmun Rev 15(7):726–735

Gilhar A, Keren A, Paus R (2019a) JAK inhibitors and alopecia areata. Lancet 393(10169):318–319

Gilhar A, Laufer-Britva R, Keren A, Paus R (2019b) Frontiers in alopecia areata pathobiology research. J Allergy Clin Immunol 144(6):1478–1489

Giordano CN, Sinha AA (2013) Cytokine pathways and interactions in alopecia areata. Eur J Dermatol 23(3):308–318

Hamed FN, Åstrand A, Bertolini M, Rossi A, Maleki-Dizaji A, Messenger AG, McDonagh AJG, Tazi-Ahnini R (2019) Alopecia areata patients show deficiency of FOXP3+CD39+ T regulatory cells and

clonotypic restriction of Treg TCRβ-chain, which highlights the immunopathological aspect of the disease. PLoS One 14(7):e0210308
Harris JE (2013) Vitiligo and alopecia areata: apples and oranges? Exp Dermatol 22(12):785–789
Ito T (2010) Hair follicle is a target of stress hormone and autoimmune reactions. J Dermatol Sci 60:67–73
Ito T, Ito N, Bettermann A, Tokura Y, Takigawa M, Paus R (2004) Collapse and restoration of MHC Class-I-dependent immune privilege. Am J Pathol 164(2):623–634
Ito N, Ito T, Kromminga A, Bettermann A, Takigawa M, Kees F, Straub RH, Paus R (2005) Human hair follicles display a functional equivalent of the hypothalamic-pituitary-adrenal axis and synthesize cortisol. FASEB J 19(10):1332–1334
Ito T, Ito N, Saathoff M, Bettermann A, Takigawa M, Paus R (2005) Interferon-γ is a potent inducer of catagen-like changes in cultured human anagen hair follicles. Br J Dermatol 152(4):623–631
Ito T, Ito N, Saathoff M, Hashizume H, Fukamizu H, Nickoloff B, Takigawa M, Paus R (2008) Maintenance of hair follicle immune privilege is linked to prevention of NK cel lattack. J Invest Dermatol 128(5):1196–1206
Ito T, Hashizume H, Shimauchi T, Funakoshi A, Ito N, Fukamizu H, Takigawa M, Tokura Y (2013) CXCL10 produced from hair follicles induces Th1 and Tc1 cell infiltration in the acute phase of alopecia areata followed by sustained Tc1 accumulation in the chronic phase. J Dermatol Sci 69:140–147
Jensen O, Pannbacker VO, Mosekilde E, Dewel G, Borckmans P (1994) Localized structures and front propagation in the Lengyel–Epstein model. Phys Rev E 50(2):736–749
Jimbo H, Nagai H, Fujiwara S, Shimoura N, Nishigori C (2020) Fas-FasL interaction in cytotoxic T cell-mediated vitiligo: the role of lesional expression of tumor necrosis factor-α and interferon-γ in Fas-mediated melanocyte apoptosis. Exp Dermatol 29(1):61–70
Jimenez F, Ruifernández JM (1999) Distribution of human hair in follicular units. A mathematical model for estimating the donor size in follicular unit transplantation. Dermatol Surg 25(4):294–298
Kang H, Wu WY, Yu M, Shapiro J, McElwee KJ (2019) Increased expression of TLR7 and TLR9 in alopecia areata. Exp Dermatol. https://doi.org/10.1111/exd.14043
Keller EF, Segel LA (1971) Model for chemotaxis. J Theor Biol 30:225–234
Kinori M, Bertolini M, Funk W, Samuelov L, Meyer KC, Emelianov VU, Hasse S, Paus R (2012) Calcitonin gene-related peptide (CGRP) may award relative protection from interferon-induced collapse of human hair follicle immune privilege. Exp Dermatol 21(3):223–226
Krummel MF, Bartumeus F, Gérard A (2016) T-cell migration, search strategies and mechanisms. Nat Rev Immunol 16(3):193–201
Li J, van Vliet C, Rufaut NW, Jones LN, Sinclair RD, Carbone FR (2016) Laser capture microdissection reveals transcriptional abnormalities in alopecia areata before, during, and after active hair loss. J Invest Dermatol 136(3):715–718
Luster AD, Ravetch JV (1987) Biochemical characterization of a gamma interferon-inducible cytokine (IP-10). J Exp Med 166(4):1084–1097
McElwee KJ, Gilhar A, Tobin DJ, Ramot Y, Sundberg JP, Nakamura M, Bertolini M, Inui S, Tokura Y, King LE Jr, Duque-Estrada B, Tosti A, Keren A, Itami S, Shoenfeld Y, Zlotogorski A, Paus R (2013) What causes alopecia areata? Exp Dermatol 22:609–626
Mohri H, Perelson AS, Tung K, Ribeiro RM, Ramratnam B, Markowitz M, Kost R, Hurley A, Weinberger L, Cesar D, Hellerstein MK, Ho DD (2001) Increased turnover of T lymphocytes in HIV-1 infection and its reduction by antiretroviral therapy. J Exp Med 194(9):1277–1287
Murray JD (2003a) 2. Spatial pattern formation with reaction diffusion systems. In: Antman SS, Marsden JE, Sirovich L, Wiggins S (eds) Mathematical biology II: spatial models and biomedical applications, 3rd edn. Springer, Berlin
Murray JD (2003b) 3. Animal coat patterns and other practical applications of reaction diffusion mechanisms. In: Antman SS, Marsden JE, Sirovich L, Wiggins S (eds) Mathematical biology II: spatial models and biomedical applications, 3rd edn. Springer, Berlin
Murray JD (2003c) 4. Pattern formation on growing domains: alligators and snakes. In: Antman SS, Marsden JE, Sirovich L, Wiggins S (eds) Mathematical biology II: spatial models and biomedical applications, 3rd edn. Springer, Berlin
Murray JD (1981) A pre-pattern formation mechanism for animal coat markings. J Theor Biol 88:161–199
Myerscough MR, Murray JD (1992) Analysis of propagating pattern in a chemotaxis system. Bull Math Biol 54(1):77–94
Paus R, Cotsarelis G (1999) The biology of hair follicles. N Engl J Med 341(7):491–497

Paus R, Slominski A, Czametzki BM (1993) Is alopecia areata an autoimmune-response against melanogenesis-related proteins, exposed by abnormal MHC class I expression in the anagen hair bulb? Yale J Biol Med 66:541–554

Paus R, Nickoloff BJ, Ito T (2005) A 'hairy' privilege. Trends Immunol 26(1):32–40

Paus R, Arck P, Tiedea S (2008) (Neuro-)endocrinology of epithelial hair follicle stem cells. Mol Cell Endocrinol 288:38–51

Paus R, Bulfone-Paus S, Bertolini M (2018) Hair follicle immune privilege revisited: the key to alopecia areata management. J Invest Dermatol Symp Proc 19(1):S12–S17

Peters EMJ, Liotiri S, Bodó E, Hagen E, Bíró T, Arck PC, Paus R (2007) Probing the effects of stress mediators on the human hair follicle. Substance P holds central position. Am J Pathol 171(6):1872–1886

Petukhova L, Duvic M, Hordinsky M, Norris D, Price V, Shimomura Y, Kim H, Singh P, Lee A, Chen W, Meyer K, Paus R, Jahoda C, Amos C, Gregersen P, Christiano A (2010) Genome-wide association study in alopecia areata implicates both innate and adaptive immunity. Nature 466:113–117

Picardo M, Taïeb A (2019) Focus theme issue: "vitiligo and other pigmentary disorders". Exp Dermatol 28(6):639–641

Pigozzo AB, Macedo GC, dos Santos RW, Lobosco M (2011) Implementation of a computational model of the innate immune system. In: ICARIS proceedings. Artificial immune systems, pp 95–107

Plikus MV, Van Spyk EN, Pham K, Geyfman M, Kumar V, Takahashi JS, Andersen B (2015) The circadian clock in skin: implications for adult stem cells, tissue regeneration, cancer, aging, and immunity. J Biol Rhythms 30(3):163–82

Rork JF, Rashighi M, Harris JE (2016) Understanding autoimmunity of vitiligo and alopecia areata. Curr Opin Pediatr 28(4):463–469

Rose NR, Mackay I (eds) (2013) Autoimmune disease: the consequence of disturbed homeostasis. In: The autoimmune diseases, 5th edn. Academic Press, New York, pp 3–9

Rot A, von Andrian UH (2004) Chemokines in innate and adaptive host defense: basic chemokinese grammar for immune cells. Annu Rev Immunol 22:891–928

Schneider MR, Schmidt-Ullrich R, Paus R (2009) The hair follicle as a dynamic miniorgan. Curr Biol 19(3):R132–R142

Segel LA (1984) Modeling dynamic phenomena in molecular and cellular biology, 1st edn. Cambridge University Press, Cambridge

Skurkovich B, Skurkovich S (2003) Anti-interferon-gamma antibodies in the treatment of autoimmune diseases. Curr Opin Mol Ther 5(1):52–57

Speiser JJ, Mondo D, Mehta V, Marcial SA, Kini A, Hutchens KA (2019) Regulatory T-cells in alopecia areata. J Cutan Pathol 46(9):653–658

Thelen M, Uguccioni M (2016) Volume 2: Molecular immunology. In: Ratcliffe MJH, Colonna M, Elliott T, Mantovani A, Martin A (eds) Cytokines and their receptors. Function of chemokines and their receptors in immunity, Encyclopedia of immunobiology, 1st edn. Elsevier, Amsterdam, pp 572–578

Ujiie H (2019) Regulatory T cells in autoimmune skin diseases. Exp Dermatol 28(6):642–646

Wańkowicz-Kalińska A, van den Wijngaard RM, Tigges BJ, Westerhof W, Ogg GS, Cerundolo V, Storkus WJ, Das PK (2003) Immunopolarization of CD4+ and CD8+ T cells to Type-1-like is associated with melanocyte loss in human vitiligo. Lab Invest 83(5):683–695

Widelitz RB, Baker RE, Plikus M, Lin CM, Maini PK, Paus R, Chuong CM (2006) Distinct mechanisms underlie pattern formation in the skin and skin appendages. Birth Defects Res C Embryo Today 78(3):280–291

Xing L, Dai Z, Jabbari A, Cerise JE, Higgins CA, Gong W, deJong A, Harel S, DeStefano GM, Rothman L, Singh P, Petukhova L, Mackay-Wiggan J, Christiano AM, Clynes R (2014) Alopecia areata is driven by cytotoxic T lymphocytes and is reversed by JAK inhibition. Nat Med 20:1043–1049

Affiliations

Atanaska Dobreva[1] · Ralf Paus[2,3,4] · N. G. Cogan[5]

✉ Atanaska Dobreva
azdobrev@ncsu.edu

1 Department of Mathematics, North Carolina State University, 2108 SAS Hall, 2311 Stinson Drive, Raleigh, NC 27695, USA

2 Dr. Phillip Frost Department of Dermatology and Cutaneous Surgery, University of Miami Miller School of Medicine, Miami, FL 33136, USA

3 Centre for Dermatology Research, University of Manchester and NIHR Manchester Biomedical Research Centre, Manchester, UK

4 Monasterium Laboratory, Muenster, Germany

5 Department of Mathematics, Florida State University, 208 Love Building, 1017 Academic Way, Tallahassee, FL 32306, USA